Chin.J.Geochem.(2013)32:337–346
DOI: 10.1007/s11631-013-0641-3

Geochemistry and petrogenesis of Late Ladinian OIB-like basalts from Tabai, Yunnan Province, China

ZHANG Jiawei[1,2], HUANG Zhilong[1*], LUO Taiyi[1], QIAN Zhikuan[1,2], and ZHANG Ying[1,2]

[1] *State Key Laboratory of Ore Deposit Geochemistry, Institute of Geochemistry, Chinese Academy of Sciences, Guiyang 550002, China*

[2] *University of the Chinese Academy of Sciences, Beijing 100039, China*

[*] *Corresponding author, E-mail: huangzhilong@vip.gyig.ac.cn*

Received July 8, 2012; accepted August 8, 2012

Abstract Major and trace elements analysis has been carried out on the Late Ladinian Tabai basalts from Yunnan Province with the aim of studying their petrogenesis. Their SiO_2 contents range from 43.63 wt.% to 48.23 wt.%. The basalts belong to the weakly alkaline (average total alkalis Na_2O+K_2O=3.59 wt.%), high-Ti (3.21 wt.% to 4.32 wt.%) magma series. The basalts are characterized by OIB-like trace elements patterns, which are enriched in large ion lithosphile elements (LILE) including Rb and Ba, and display negative K, Zr and Hf anomalies as shown on the spider diagrams. The Tabai basalts display light rare-earth elements (LREE) enrichment and are depleted in heavy rare-earth elements (HREE) on the REE pattern. Those dates indicate that the parental magma of the Tabai basalts was derived from low-degree (1%–5%) partial melting of garnet peridotite. The magma underwent olivine fractional crystallization and minor crustal contamination during their ascent. The Tabai basalts were related to a relaxation event which had triggered the Emeishan fossil plume head re-melting in the Middle Triassic.

Key words OIB; high-Ti basalt; petrogenesis; Tabai; SW China

1 Introduction

In the Gejiu tin ore district, located near the city of Gejiu, in the southeastern part of Yunnan Province, there occurs primarily a super large-scale tin ore deposit but also a copper-rich polymetallic ore deposit containing Cu, Pb, Zn, Ag, Fe, S, W, Bi and In (Zhuang Yongqiu et al., 1996). Significant exploration has been performed by local geologists since 1950. It led to the discovery of several large deposits, including the Songshujiao, Laochang and Kafang deposits in the eastern part of the study area.

There were three periods of basaltic lava eruption in the Gejiu area during the Triassic (Li Yingshu et al., 2009a): (1) the Anisian basalts; (2) the Early Ladinian basalts; and (3) the Late Ladinian basalts. The Anisian basalts are hosted in the lower part of the Gejiu Formation (T_2g_1). Those basalts are mainly located deeply underground at Kafang and Laochang and exposed at Qilinshan in the eastern part of the Gejiu district. The Early Ladinian basalts occur in the lower part of the Falang Formation and the Late Ladinian basalts occur in the upper part of the Falang Formation in the western part of the Gejiu district.

The petrology and geochemistry of the Kafang and Laochang Anisian basalts were well documented (Li Yingshu et al., 2009b; Zhang Hai et al., 2009; Fang Weixuan and Jia Runxing, 2011). Beside the traditional granite metallogenic theory (Mao Jingwen et al., 2008; Cheng Yanbo and Mao Jingwen, 2010), some geoscientists (Zhang Huan et al., 2007; Li Yingshu et al., 2006; 2009c) supposed that the primitive metallogenic source beds could exist at the time when the Kafang and Laochang basalts erupted before the granitic intrusions superimposed on them.

Unlike the Anisian basalts, the origin of the Late Ladinian Tabai basalts is poorly understood and their petrogenesis is still unknown due to the lack of sys-

temic studies here. A detailed investigation is longing to investigate the petrology and geochemistry of the Tabai basalts in order to constrain their sources, to reveal the tectonic setting during magma eruption and to understand the temporal evolution relationship between the Anisian basalts and the Late Ladinian basalts.

In this study, the major and trace element geochemistry data of the Tabai basalts were reported and we used these data to investigate the factors controlling the petrogenesis of the Tabai basalts, including their source(s), the degree of partial melting and subsequent crystal fractionation and crustal contamination.

2 Geological setting and petrography of the Tabai basalts

2.1 Geological setting

The Gejiu district is distributed along the suture zone of the Indian Plate and the Eurasian Plate on the western margin of the Youjiang fold belt (Fig. 1). This district has undergone a prolonged history of tectonism and complex structural activity, resulting in varying-scale fault and fold systems. The NS-trending Gejiu fault divides the Gejiu area into two parts, eastern and western. The NW-trending Baishachong fault in the eastern part and three NNE-trending faults named Longchahe, Jiaodingshan and Yangjiatian, respectively in the western part are the main structures in the area. Several parallel E-W trending and two N-E trending faults in the eastern part control the general configuration of the mineralization and distribution of orebodies in the Gejiu district (Fig. 2).

Throughout the Middle Triassic, the dominant strata (over 3000 m) are the Gejiu Formation (T_2g) and the Falang Formation (T_2f). They were formed by a long-life depression. The Gejiu Formation consists mainly of carbonates and the Falang Formation is made up of sandstones and shales.

The Triassic lavas were widely distributed in the Gejiu area. The copper deposit-related Anisian basalts are hosted in the lower part of the Gejiu Formation in the eastern part. The Early Ladinian basalts are hosted in the lower part of the Falang Formation and the Late Ladinian basalts occur in the upper part of the Falang Formation in the western part of the Gejiu district. This paper focuses on the Late Ladinian basalts.

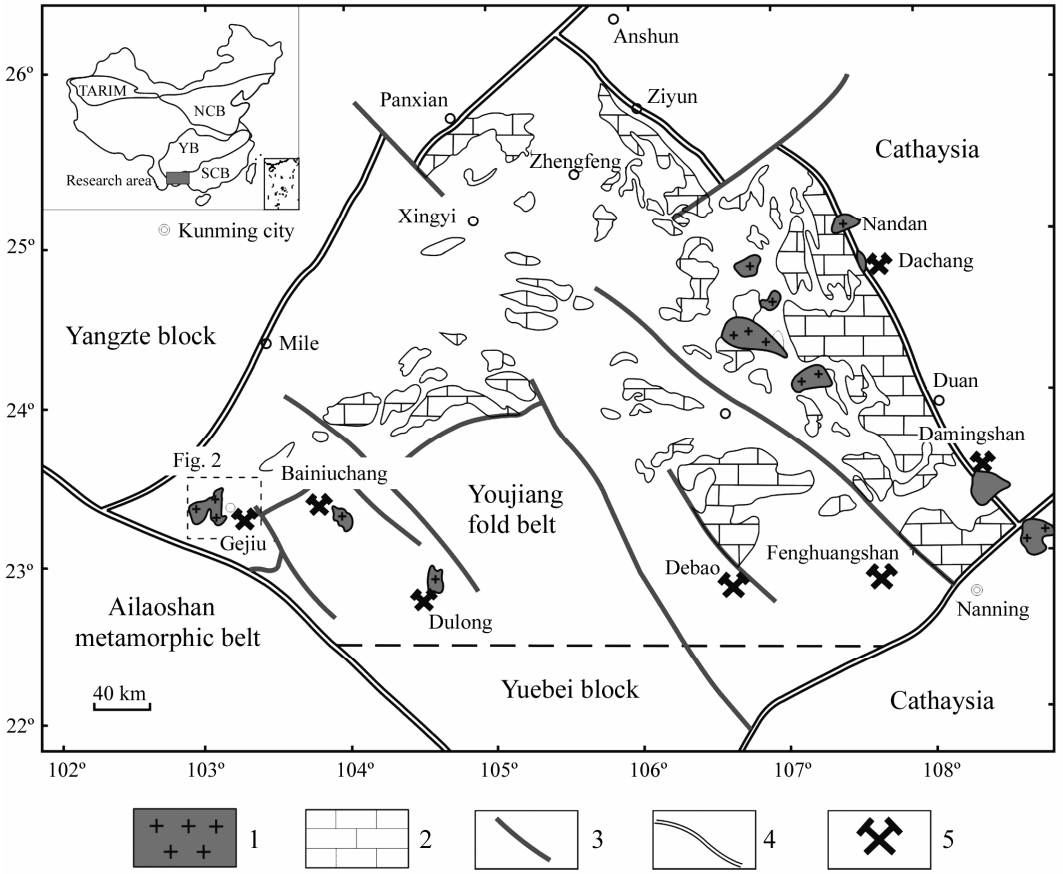

Fig. 1. The distribution of structures and deposits in the Youjiang fold belt and the locations of surrounding tectonic units (modified after Zhang Yin et al., 2011). 1. Granite; 2. carbonate; 3. fault; 4. geological unit boundary; 5. tin deposit.

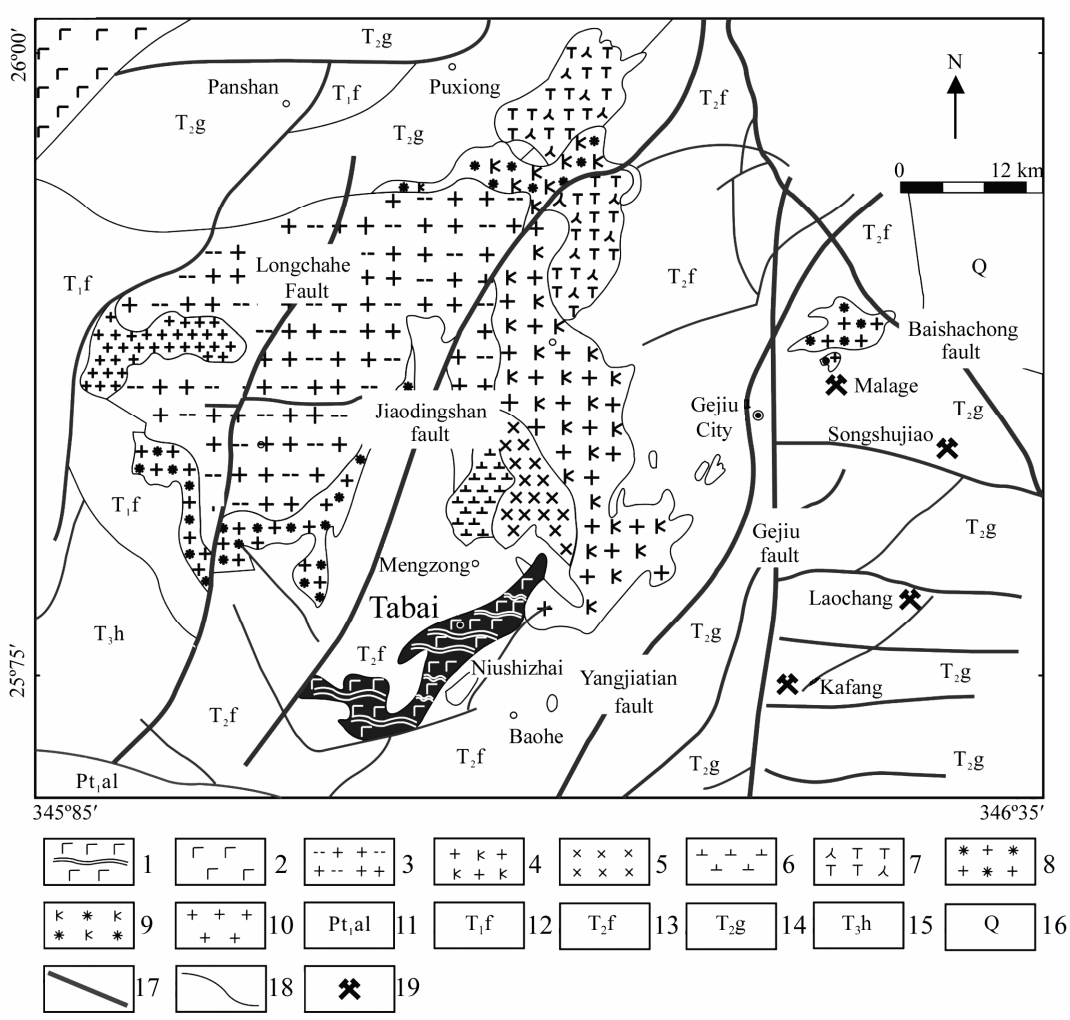

Fig. 2. The geologic map of the Gejiu area, Yunnan Province (modified after Zhang Yin et al., 2011). 1.Tabai basalt; 2. Emeishan basalt; 3. phyric granite; 4. alkali feldspar granite; 5. granite; 6. diorite; 7. syenite; 8. alkali granite; 9. sienite; 10. granite; 11. Ailaoshan metamorphic belt; 12. Falang Formation; 13. Feixianguan Formation; 14. Gejiu Formation; 15. Huobachong Formation; 16. Quaternary; 17. fault; 18. geologic unit boundary; 19. ore deposit.

Besides the Triassic lavas, the Mesozoic igneous rocks were emplaced in both eastern and western parts of the Gejiu district within a short period, from 76 to 85 Ma (Cheng Yanbo and Mao Jingwen, 2010). The granite intrusion was emplaced at the Gejiu Formation deeply underground in the eastern part and the Jiaodingshan fault has controlled the distribution of magmatic rocks in the western part of the Gejiu area.

2.2 Petrography and sampling

The Tabai basalts were emerged in the southern part of Mengzong Village, mainly around Tabai and Niushizhai Villages. Those basalts are stratiform (Fig. 3a), conformably contacted with the Falang Formation as revealed from field observation (Fig. 3b) and extend in the NE-direction with an area of 40 km^2 in space, with a maximal thickness of about 1700 m. The samples were collected from the road side between Gejiu City and Mengzong Village where the best outcrops were observed. The representative fresh samples were collected and labeled at every 200-meters interval. The hand specimens of Tabai basalts were dark green in color and exhibited massive structure in general. Black and green minerals in some samples showed alternate layers (Fig. 3c) and some contained a small quantity of quartz amygdaloids and quartz veins (Fig. 3c, d).

The Tabai basalts exhibited blastoporphyritic texture as evidenced from the microphotographs (Fig. 4a, b). The phenocrysts (5%–10%) were mostly olivine and some showed kink bands. Minerals in the Tabai basalts had suffered strong alteration. Chlorite was an alteration product of dark minerals such as olivine and pyroxene. Meanwhile part of plagioclase turned into hydrosialite. The groundmass of these minerals exhibited oriented structure (Fig. 4c). The main rock-forming minerals of the Tabai basalts after

CIPW norm mineral calculation (Table 1) are plagioclase (60%–65%), pyroxene (10%–30%), olivine (5%–15%) and Fe-Ti oxide (7%).

3 Analytical procedure

A detailed petrographic examination was carried out on the studied samples in order to avoid the effects of secondary alteration and weathering. The samples were crushed manually and powered by means of an agate mortar for the following analyses.

3.1 Whole-rock major and trace element analysis

Seven samples were chosen for whole-rock major, trace element and ferrous Fe analysis at ALS Laboratory Group, Guangzhou, China.

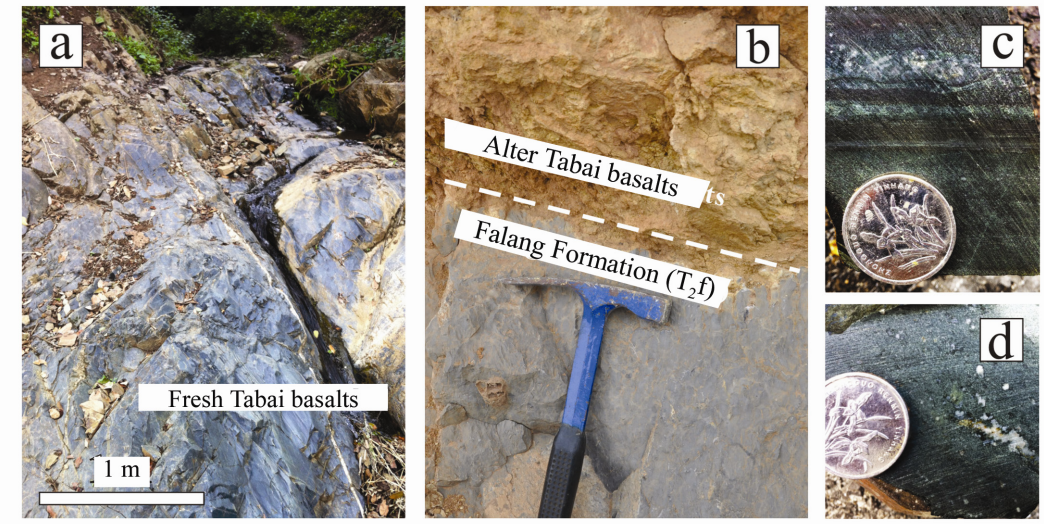

Fig. 3. Outcrops and hand specimens of the Tabai basalts.

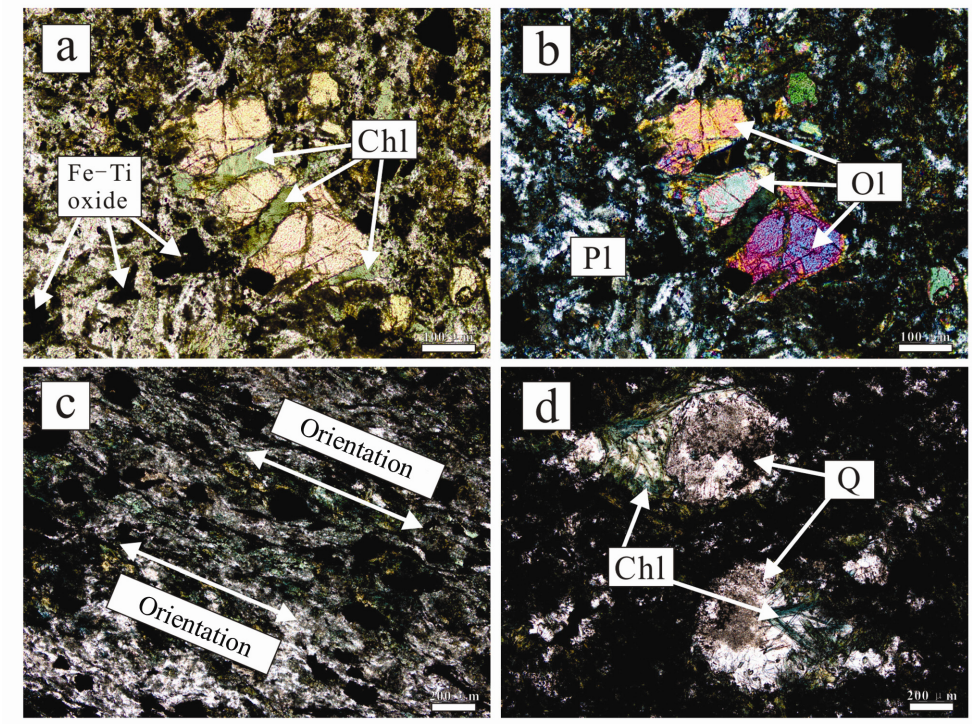

Fig. 4. Microphotographs of the Tabai basalts.

A calcined or ignited sample for major element analysis (0.9 g) was added to 9.0 g of Lithium Borate Flux (50%–50% $Li_2B_4O_7$-$LiBO_2$), mixed well and fused in an auto fluxer between 1050–1100℃. A flat molten glass disc was prepared from the resulting melt. This disc was then analyzed by X-ray fluorescence spectrometry. The relative standard deviation (RSD) and the relative error (RE) were lower than 2%.

In terms of the trace elements analytical process, the sample was added to lithium metaborate flux, mixed well and fused in a furnace at 1000℃. The resultant melt was then cooled and dissolved in 100 mL of 4% HNO_3/2% HCl solution. This solution was then analyzed by inductively coupled plasma mass spectrometry. The relative standard deviation (RSD) and the relative error (RE) were lower than 5%.

3.2 Ferrous Fe analysis

Ferrous Fe was measured in order to calculate the precise Mg numbers (not hypothetical) of basalts. Because the calculation of Mg numbers needs to acquire the real ferrous Fe contents in the basalts but most of them only had ferric Fe contents, assuming $FeO=0.89\times Fe_2O_3$. The ferrous Fe was determined by acid decomposition and titration with potassium dichromate. A prepared sample was digested with sulphuric and hydrofluoric acids. The sample solution containing ferrous iron was then titrated in a beaker containing diluted sulphuric acid, orthophosphoric acid and boric acid with potassium dichromate solution. The lower limit of this method was 0.01%.

4 Results

4.1 Major elements

Most of the basalt samples were correlated to the alkaline series basalts based on the total alkali-silica (TAS) comparison (Fig. 5). The SiO_2 contents (recalculated to 100 wt.%) of all basalt samples varied between 43.63 wt.%–48.23 wt.% and had TiO_2 contents greater than 3.2 wt.% (ranging from 3.21 wt.% to 4.32 wt.%), consistent with previous identification as the Emeishan high-Ti series basalts (Wang Yan et al., 2007). In addition, all the basalts samples had distinctly high contents of Fe_2O_3 (14.34 wt.%–20.73 wt.%), Al_2O_3 (13.80 wt.%–15.44 wt.%), CaO (5.73 wt.%–10.47 wt.%) and Na_2O (1.91 wt.%–3.93 wt.%), but relatively low contents of MgO (4.08 wt.%–5.91 wt.%), low Mg numbers (46–53) and K_2O (0.15 wt.%–1.91 wt.%) as listed in Table 1.

4.2 Trace elements

In the primitive mantle-normalized diagram (Fig. 6a), the Tabai basalts display LILE-enrichment patterns and show remarkably negative Zr, Hf and K anomalies, strongly positive Pb anomalies and slightly negative U and Sr anomalies. The basalts display uniform chondrite-normalized LREE-enrichment patterns with no Ce and Eu anomalies (Fig. 6b). Their $(La/Yb)_N$ (primitive mantle normalized) ratios range from 12.29 to 18.77 and $(La/Sm)_N$ from 2.39 to 2.90. To sum up, these unique patterns are very similar to those of the Emeishan high-Ti basalts as reported by Lai Shaocong et al. (2011).

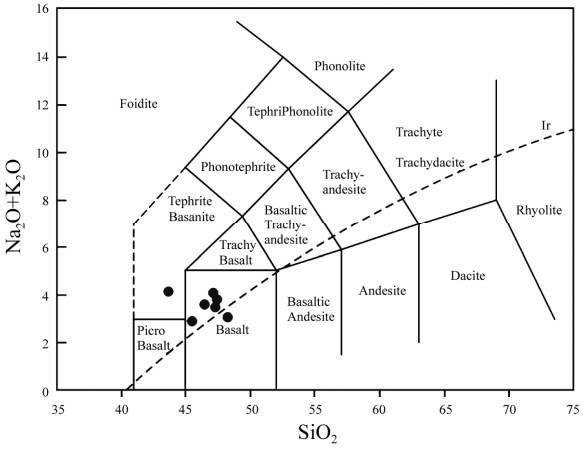

Fig. 5. Total alkali-silica (TAS) diagram of the Tabai basalt samples. Dotted line distinguishes alkaline basalts from subalkaline basalts (after Le Bas, 1986).

5 Discussion

5.1 Alteration

The low LOI (<4%) of the Tabai basalt samples indicated relatively weak weathering. However, the physical and chemical alterations still occurred due to the appearance of chlorite and hydrosialite in microphotographs and variable concentrations of mobile elements such as Rb, Ba and Sr (Fig. 6). In contrast, both high field strength elements (HFSE) and REE typically remained immobile during metamorphism or hydrothermal alteration. The ratios of these elements remained constant. Therefore, the concentrations of HFSE and REE reported here were thus assumed to represent suitable proxies by which we can evaluate the petrogenesis of the basalts (Staudigel and Hart, 1983; Wang Yan et al., 2007).

5.2 Fractional crystallization and crustal contamination

The MgO contents of the Tabai basalt samples range from 4.08 wt.% to 5.91 wt.% and Mg numbers range from 46 to 53, suggesting that the basalts could have experienced magma evolution prior to the eruption of the lavas compared to the Mg numbers (68–72) of primitive basaltic magma (Green, 1976). The fractionation processes (AFC or FC processes) could be identified by SiO_2 vs. Nb/La plots (Fig. 7). AFC process will enhance the contents of SiO_2 and reduce HFSE (such as Nb), causing lower Nb/La ratios. In contrast, FC processes did not change the Nb/La ratios (Ernst et al., 1988; Xiao Long et al., 2008). In Fig. 7, a constant Nb/La ratio for all samples suggests that there was no significant AFC process but that FC occurred.

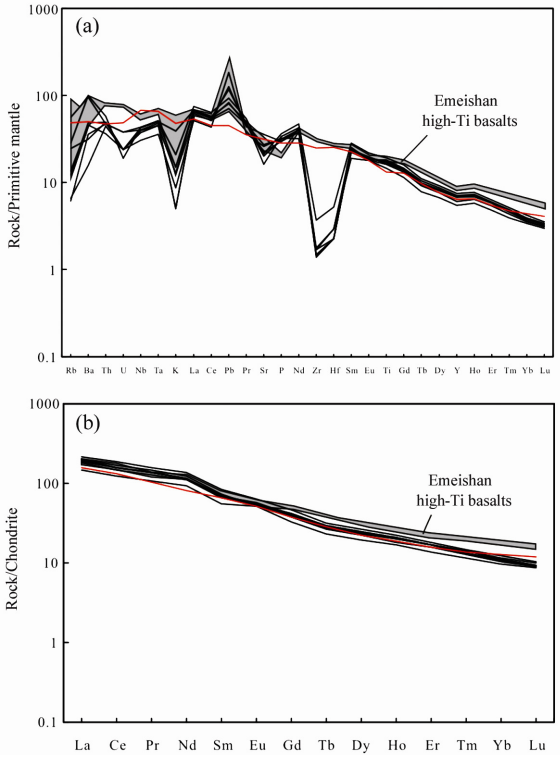

Fig. 6. Primitive mantle-normalized trace element patterns (a) and chondrite-normalized REE patterns (b) of the Tabai basalts. Normalization and OIB (red line) values followed by Sun and McDonough (1989) and the Emeishan high-Ti basalts followed by Lai Shaocong et al. (2011).

The low abundances of the iron-group elements Cr (15×10^{-6}–60×10^{-6}), Co (60×10^{-6}–72×10^{-6}) and Ni (41.8×10^{-6}–76×10^{-6}) observed in the Tabai basalts indicated significant fractionation of olivine and clinopyroxene (Arth, 1976). The presence of olivine phenocrysts in most samples also gave a support to early crystallization of this mineral.

In the primitive mantle normalized trace element patterns (Fig. 6), the Tabai basalts showed remarkably positive Pb anomalies, indicating that crustal contamination once happened. Both $(Nb/La)_{PM}$ and $(Th/Nb)_{PM}$ ratios (normalized to the primitive mantle) were good proxies for crustal contamination (Wang Yan et al., 2007). Nb generally was low in concentrations in the crust while La was typically enriched in the crust. Th was commonly enriched in sediments. $(Nb/La)_{PM}$ ratios in the Tabai basalts (0.57–0.63) were lower than the values expected for the primitive mantle (Nb/La=1.04) while the $(Th/Nb)_N$ ratios (1.09–1.33) were close to the values expected for the primitive mantle (Th/Nb=1.20). This indicated the occurrence of slight crustal assimilation. On the Ce/Pb vs. Ce plot (Fig. 8b), Ce/Pb ratios in the Tabai basalts are lower than the average value of OIB (25±5) as reported by Hofmann et al. (1986). Again, this indicated that crustal contamination took place during the ascending of the Tabai basalts.

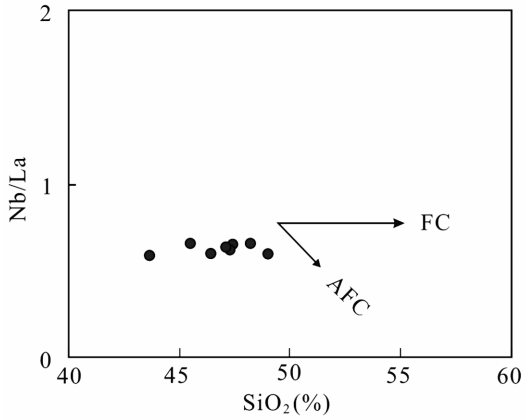

Fig. 7. Nb/La versus SiO_2 plot (after Ernst et al., 1988).

5.3 Mantle source, partial melting and plume indications

From the former studies it was believed that it is feasible to trace the mantle source of basalts by using immobile incompatible elements, or better yet, immobile incompatible element ratios (Weaver, 1991; Fitton et al., 1997; Baksi, 2001; Condie, 2003; Fitton et al., 2003; Condie, 2005; Willbold and Stracke, 2006; Pearce, 2008).

In the Nb/Yb vs. TiO_2/Yb plot (Pearce, 2008), all of the Tabai basalts fall in the area of OIB, suggesting the Tabai basalts had the same source as OIB did, which came from the enriched mantle. Besides, most of the samples had Nb/U values basically similar to the value range of OIB (Nb/U=47±10) (Fig. 8a), higher than those of the primitive mantle (Nb/U–30) and the continental crust (Nb/U≈10) (Hofmann et al., 1986), suggesting its plume origin.

Table 1 Major, trace elements and CIPW Norm mineral calculation of Tabai basalts

Sample	11TB-5	11TB-6	11TB-8	11TB-9	11TB-10	11TB-11	11TB-14
Major elements (recalculated to 100 wt.% on a volatile-free basis)							
SiO_2	46.44	45.51	47.40	48.23	47.28	43.63	47.12
TiO_2	3.62	3.76	3.84	3.97	3.21	4.32	3.54
Al_2O_3	14.87	14.90	14.52	13.80	14.28	15.44	13.91
Fe_2O_3	17.52	17.24	17.26	15.96	14.34	20.73	16.34
MnO	0.29	0.24	0.28	0.27	0.21	0.24	0.29
MgO	5.89	5.59	5.62	5.91	5.32	4.08	5.09
CaO	6.92	9.10	6.32	7.80	10.47	5.73	8.70
Na_2O	3.20	2.44	3.65	1.91	3.25	3.50	3.93
K_2O	0.39	0.46	0.15	1.19	0.26	0.65	0.15
P_2O_5	0.65	0.67	0.67	0.72	0.69	0.78	0.64
Total	99.79	99.91	99.71	99.76	99.31	99.10	99.73
LOI	1.97	1.23	1.99	1.65	0.93	3.03	1.47
FeO	9.42	10.60	9.08	9.92	9.86	8.62	10.90
Minerals (Vol. %)							
Quartz	0	0	0	3.84	0	0	0
Plagioclase	61.0	57.4	62.8	48.4	59.4	63.0	62.1
Orthoclase	2.8	3.3	1.1	8.6	1.9	4.8	1.1
Corundum	0	0	0	0	0	0.34	0.0
Diopside	3.9	9.7	3.2	6.5	18.3	0.0	14.7
Hypersthene	17.1	16.5	19.8	24.7	6.6	8.3	3.5
Olivine	7.8	5.4	5.1	0.0	6.9	14.4	11.3
Ilmenite	4.6	4.7	4.8	5.0	4.0	5.5	4.4
Magnetite	1.6	1.5	1.5	1.4	1.3	1.9	1.4
Apatite	1.5	1.5	1.5	1.6	1.6	1.8	1.5
Total	100.0	100.0	100.0	100.0	100.0	100.0	100.0
Trace element ($\times10^{-6}$)							
Sc	26.1	26.7	27.4	27.6	28.2	30.0	25.2
V	396	398	407	366	349	397	374
Cr	15	18	18	16	60	20	15
Co	72	70	65	64	60	61	62
Ni	41.9	49.9	46.1	41.8	76.0	44.5	42.6
Cu	106.5	89.2	67.8	48.0	95.6	35.1	65.0
Zn	180	167	161	176	107	149	151
Ga	22.8	24.0	22.7	20.7	20.3	27.1	22.1
Cs	0.78	1.31	0.62	1.91	0.89	1.37	0.55
Rb	7.8	15.5	3.9	35.8	8.6	17.9	4.2
Ba	340	220	250	670	320	700	110
Th	4.2	4.2	4.0	4.0	3.1	4.9	3.8
U	0.5	0.5	0.8	0.8	0.5	0.4	0.5
Nb	28.1	30.3	28.8	30.8	21.8	30.8	26.8
Ta	1.86	2.05	1.95	2.05	1.47	2.12	1.84
Pb	5.9	8.3	5.0	5.7	13.1	6.6	9.0
Sr	466	425	572	339	551	446	760
Zr	15.5	16.0	16.5	19.8	18.9	41.2	18.8
Hf	0.7	0.7	0.7	0.9	0.9	1.6	0.7
Y	31.0	30.7	30.8	32.2	24.8	34.3	27.5
La	47.1	46.3	44.2	46.8	35.1	51.7	42.3
Ce	97.9	98.0	96.0	102.5	76.6	113.0	91.2
Pr	12.90	12.95	12.80	13.75	10.05	14.95	12.05
Nd	54.4	54.3	54.5	57.7	43.2	63.4	51.0
Sm	10.50	10.50	10.70	11.25	8.39	12.65	9.90
Eu	3.34	3.16	3.22	3.03	3.00	3.68	3.06
Gd	8.27	8.14	8.56	8.69	6.79	9.54	7.85
Tb	1.03	1.05	1.07	1.12	0.85	1.19	0.99
Dy	6.02	5.92	6.12	6.34	4.89	6.77	5.59
Ho	1.13	1.13	1.17	1.19	0.94	1.26	1.04
Er	2.75	2.79	2.82	2.83	2.30	3.03	2.57
Tm	0.34	0.34	0.36	0.36	0.29	0.38	0.32
Yb	1.80	1.86	1.87	1.93	1.66	2.08	1.73
Lu	0.23	0.24	0.24	0.25	0.22	0.26	0.23
Ratios							
Mg number	53	48	52	51	49	46	45
Nb/U	56	61	36	39	44	77	54
Ce/Pb	17	12	19	18	6	17	10
$(Nb/La)_{PM}$	0.57	0.63	0.62	0.63	0.59	0.57	0.61
$(Th/Nb)_{PM}$	1.25	1.16	1.17	1.09	1.19	1.33	1.19

Note: Mg number = $100\times Mg^{2+}/(Mg^{2+}+Fe^{2+})$ and Normalization values follow Sun and McDonough (1989).

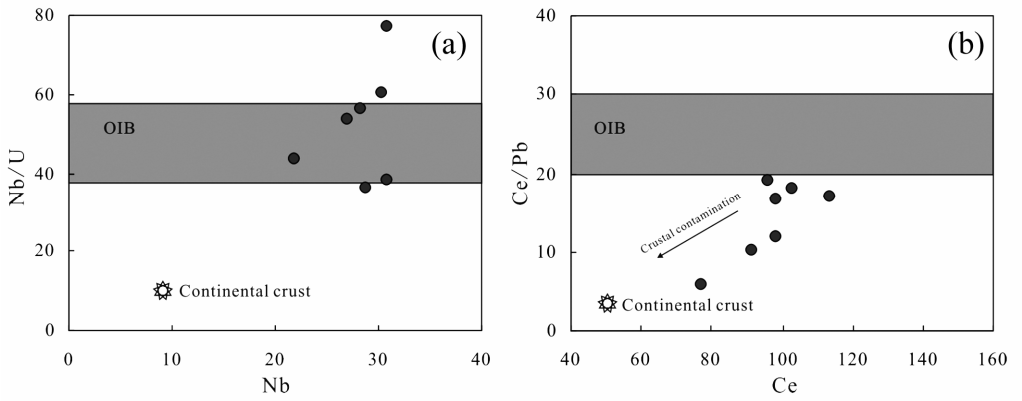

Fig. 8. Variations in trace abundances and ratios of the Tabai basalts, Nb/U vs. Nb (a) and Ce/Pb vs. Ce (b). Values of OIB and continental crust were followed by Hofmann et al. (1986).

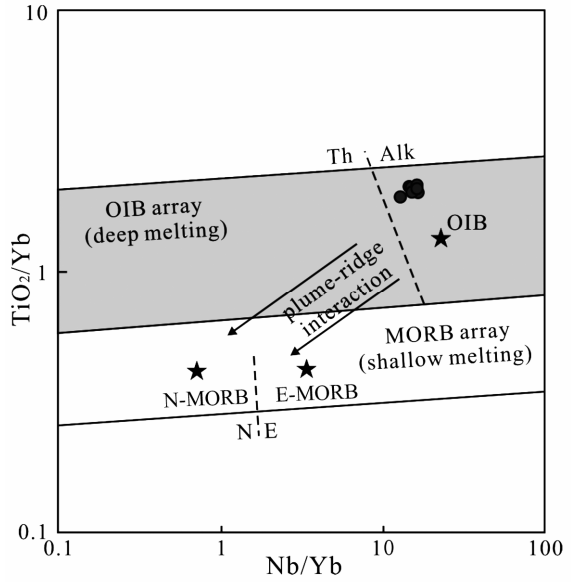

Fig. 9. The Nb/Y vs. TiO_2/Yb diagram of the source defined after Pearce (2008).

Garnet has a high partition coefficient for Y ($D_{garnet/melt}$=3.1) relative to Ti ($D_{garnet/melt}$=0.29) and Lu ($D_{garnet/melt}$=7.1) compared to La ($D_{garnet/melt}$=0.0016) (Johnson, 1998). Therefore, the high Ti/Y ratios (average of 746) and the fact of LREE enrichment and HREE depletion in the Tabai basalts are the indications of a mantle source at a garnet-stable depth.

The degree of partial melting of the mantle source could be assessed through the diagram of Sm vs Sm/Yb (Aldanmaz et al., 2000; Wang Yan et al., 2007; Qi Liang and Zhou Meifu, 2008) using the non-modal batch melting equations of Shaw (1970). According to Fig. 10, the Tabai basalts would be the products of about 1%–5% of partial melting from garnet peridotite.

5.4 Petrogenetic model

Hypotheses for OIB and OIB like basalt formation fell into three categories: (1) mantle plumes (Hofmann and White, 1982); (2) dispersed blobs or streaks of incompatible-element-enriched materials in the depleted upper mantle (Pilet et al., 2008; Niu Yaoling, 2008); and (3) a layer of shallow mantle (the perisphere; Anderson, 1995) that was enriched in incompatible elements compared to the deeper parts of the upper mantle.

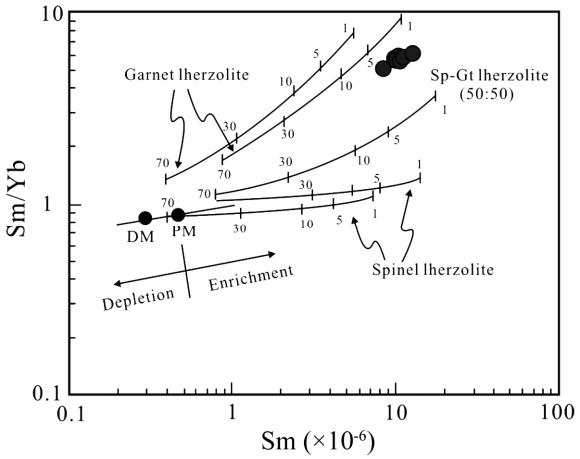

Fig. 10. Sm/Yb vs. Sm plot showing melt curves for the Tabai basalts.

The spatial location and the geochemistry similar to that of the Emeishan high-Ti basalts indicated that the Tabai basalts were related to the Emeishan plume event. However, the temporal fact that the Tabai basalts were in conformable contact with the Falang Formation excluded the possibility that the Tabai basalts resulted from the main plume event of the Emeishan flood basalts.

In consideration of the regionally geological setting and geochemistry, we proposed a feasible model to explain the generation of the Tabai basalts:

During the Middle-Late Permian, the Emeishan plume head was emplaced under western Yangzte croton, thus forming the Emeishan large igneous province (ELIP). After the quick crustal doming event

above an upwelling mantle plume (Xu Yigang et al., 2004), the plume provided the stress concentration or local weakening of the Yangtze continental lithosphere so that a post-ELIP relaxation of the Yangtze crust may occur during the Middle Triassic just as Shellnutt and Zhou (2007) and Shellnutt et al. (2008) suggested. This relaxation, in turn, made the lithosphere become thinner, induced the fossil plume head melting again and produced a small volume of Tabai magmas. Subsequently, the magmas experienced olivine fractional crystallization and some degree of crustal assimilation, finally leading to the formation of the Tabai basalts.

6 Conclusions

Combined with previous geological, petrological and geochemical studies on the basalts in the Tabai area, the following conclusions can be drawn.

(1) The Tabai basalts were derived from a low degree (1%–5%) of partial melting of agarnet peridotite mantle source. The magma experienced some degree of contamination with crustal materials and underwent fractionation of olivine prior to eruption.

(2) The Tabai basalts were one of the proxies of the magmatic events which resulted from the post-ELIP relaxation.

Acknowledgements This study is financially supported jointly by the Crisis Mines Continued Resources Exploration Project of the China Geological Survey (No. 2008186); the 12th Five-Year Plan Project of the State Key Laboratory of Ore-deposit Geochemistry, Chinese Academy of Sciences (SKLODG-ZY125-02) and the National Natural Science Foundation of China (No. 41073032). Thanks are due to Mr. Sun Hairui for geological investigation. Official reviews by Mr. Zhu Dan and language polishment by Mr. Liang Liang are gratefully appreciated.

References

Aldanmaz E., Pearce J.A., Thirlwall M.F., and Mitchell J.G. (2000) Petrogenetic evolution of Late Cenozoic, post-collisionvolcanism in western Anatolia, Turkey [J]. *Journal of Volcanology and Geothermal Research*. **102**, 67–95.

Anderson D.L. (1995) Lithosphere, asthenosphere, and perisphere [J]. *Reviews of Geophysics*. **33**, 125–149.

Arth J.G. (1976) Behavior of trace elements during magmatic processes—A summary of theoretical models and their applications [J]. *Journal of Research of the U.S. Geological Survey.* **4**, 41–47.

Baksi A.K. (2001) Search for a deep-mantle component in mafic lavas using a Nb-Y-Zr plot [J]. *Canadian Journal of Earth Sciences*. **38**, 813–824.

Cheng Yanbo and Mao Jingwen (2010) Age and geochemistry of granites in Gejiu area, Yunnan Province, SW China: Constraints on their petrogenesis and tectonic setting [J]. *Lithos*. **120**, 258–276.

Condie K.C. (2003) Incompatible element ratios in oceanic basalt and komatiites: Tracking deep mantle sources and continental growth rates with time [J]. *Geochemistry Geophysics Geosystems.* **4**.

Condie K.C. (2005) High field strength element ratios in Archean basalt: A window to evolving sources of mantle plumes [J]. *Lithos*. **79**, 491–504.

Ernst R.E., Fowler A.D., and Pearce T.H. (1988) Modeling of igneous fraction and other processes using Pearce diagrams [J]. *Contributions to Mineralogy and Petrology.* **100**, 12–18.

Fang Weixuan and Jia Runxing (2011) Characteristics of the alkaline picritic volcanic rocks in the Gejiu superlarge tin-copper deposit and their continental dynamic implications [J]. *Geotectonica et Metallogenia*. **35**, 137–148 (in Chinese with English abstract).

Fitton J.G., Saunders A.D., Norry M.J., Hardarson B.S. et al. (1997) Thermal and chemical structure of the Iceland plume [J]. *Earth and Planetary Science Letters*. **153**, 197–208.

Fitton J.G., Saunders A.D., Kempton P.D., and Hardarson B.S. (2003) Does depleted mantle form an intrinsic part of the Iceland plume [J]. *Geochemistry Geophysics Geosystems,* **4**, 1–14.

Green D.H. (1976) Experimental testing of "equilibrium" partial melting of peridotite under water-saturated, high-pressure conditions [J]. *The Canadian Mineralogist.* **14**, 255–268.

Hofmann A.W. and White W.M. (1982) Mantle plumes from ancient oceanic crust [J]. *Earth and Planetary Science Letters.* **57**, 421–436.

Hofmann A.W., Jochum K.P., Seufert M., and White W.M. (1986) Nb and Pb in oceanic basalts: New constraints on mantle evolution [J]. *Earth and Planetary Science Letters.* **79**, 33–45.

Johnson K.T.M. (1998) Experimental determination of partition coefficients for rare earth and high-field-strength elements between clinopyroxene, garnet, and basaltic melt at high pressures [J]. *Contributions to Mineralogy and Petrology.* **133**, 60–68.

Le Bas M.J., Le Maitre R.W., Streckeisen A., and Zanettin B. (1986) A chemical classification of volcanic rocks based on the total alkali-silica diagram [J]. *Jourary of Petrology.* **27**, 745–750.

Lai Shaocong, Qin Jiangfeng, Li Yongfei, Li Sanzhong, and Santosh M. (2011) Permian high Ti/Y basalt from the eastern part of the Emeishan large igneous province, southwestern China: Petrogenesis and tectonic implications [J]. *Journal of Asian Earth Sciences*. **47**, 216–230.

Li Yingshu, Qin Dexian, Dang Yutao, Xue Chuandong, Tan Shucheng, and Hong Tuo (2006) Mineralizations in basalt of the Gejiu Tin Deposit in Yunnan Province [J]. *Journal of Jilin University* (Earth Science Edition). **36**, 326–335 (in Chinese with English abstract).

Li Yingshu, Qin Dexian, Guo Ningning, Luo Xi, Xie Yang, and Zou Tao (2009a) Geochemical characteristicsof the platinum-group elements of the basic volcanic rock of the late Ladinian period in West Gejiu [J]. *Nonferrous Metals*. **61**, 22–24 (in Chinese with English abstract).

Li Yingshu, Qin Dexian, Guo Ningning, Luo Xi, Zou Tao, Wan Chaoying, and Zhou Niansheng (2009b) Geotectonic setting and mineralization significance of Indo-Chinese epoch basalt in eastern Gejiu of Yunnan [J]. *Nonferrous Metals*. **61**, 104–109 (in Chinese with English abstract).

Li Yingshu, Qin Dexian, Chen Xiying, Guo Ningning, Luo Xi, Xie Yang,

and Zou Tao (2009c) Evidences of exhalative hydrotherma sedimentary mineralization of Indo-Chinese epoch of Gejiu tin-polymetallic deposits [J]. *Nonferrous Metals.* **61**, 120–125 (in Chinese with English abstract).

Mao Jingwen, Cheng Yanbo, Guo Chunli, Yang Zongxi, and Feng Jiarui (2008) Gejiu tin polymetallic orefield: Deposit model and discussion for several points concerned [J]. *Acta Geologica Sinica*. **82**, 1455–1467 (in Chinese with English abstract).

Niu Yaoling (2008) The origin of alkaline lavas [J]. *Science.* **320**, 883–884.

Pearce J.A. (2008) Geochemical fingerprinting of oceanic basalt with applications to ophiolite classification and the search for Archean oceanic crust [J]. *Lithos.* **100**, 14–48.

Pilet S., Baker M.B., and Stolper E.M. (2008) Metasomatized lithosphere and the origin of alkaline lavas [J]. *Science*. **320**, 916–919.

Qi Liang and Zhou Meifu (2008) Platinum-group elemental and Sr-Nd-Os isotopic geochemistry of Permian Emeishan flood basalt in Guizhou Province, SW China [J]. *Chemical Geology*. **248**, 83–103.

Shaw D.M. (1970) Trace element fractionation during anatexis [J]. *Geochimica et Cosmochimica Acta.* **34**, 237–243.

Shellnutt J.G. and Zhou M.F. (2007) Permian peralkaline, peraluminous and metaluminous A-type granites in the Panxi district, SW China: Their relationship to the Emeishan mantle plume [J]. *Chemical Geology*. **243**, 286–316.

Shellnutt J.G., Zhou Meifu, Yan Danping, and Wang Yanbin (2008) Longevity of the Permian Emeishan mantle plume (SW China): 1, 8 or 18 Ma [J]. *Geological Magazine*. **145**, 373–388.

Staudigel H. and Hart S.R. (1983) Alteration of basaltic glass: Mechanisms and significance for the oceanic crust-seawater budget [J]. *Geochimica et Cosmochimica Acta.* **47**, 337–350.

Sun S.S. and McDonough W.F. (1989) *Chemical and Isotopic Systematics of Oceanic Basalt: Implications for Mantle Composition and Processes* [M]. pp.313–345. Geological Society, Special Publications, London.

Wang Yan, Zhou Meifu, and Qi Liang (2007) Permian flood basalt and mafic intrusions in the Jinping (SW China)-Song Da (northern Vietnam) district: Mantle sources, crustal contamination and sulfide segregation [J]. *Chemical Geology.* **243**, 317–343.

Weaver B.L. (1991) The origin of ocean island basalt end-member compositions: Trace element and isotopic constraints [J]. *Earth and Planetary Science Letters.* **104**, 387–397.

Willbold M. and Stracke A. (2006) Trace element composition of mantle end-members: Implications for recycling of oceanic and upper and lower continental crust [J]. *Geochemistry Geophysics Geosystems.* **7**, 1–34.

Xiao Long, He Qi, Pirajno Franco, Ni Pingze, Du Jingze, and Wei Qirong (2008) Possible correlation between a mantle plume and the evolution of Paleo-Tethys Jinshajiang Ocean: Evidence from a volcanic rifted margin in the Xiaru-Tuoding area, Yunnan, SW China [J]. *Lithos*. **100**, 112–126.

Xu Yigang, He Bin, Chung Sunlin, Menzies M.A., and Frey F.A. (2004) Geologic, geochemical, and geophysical consequences of plume involvement in the Emeishan flood-basalt province [J]. *Geology.* **32**, 917.

Zhang Huan, Tong Xiang, Wu Junde, Luo Taiyi, Tao Yan, and Zhu Dan (2007) Gejiu tin-polymetallic ore deposit: An example of landing of Red sea-type submarine hydrothermal deposition [J]. *Acta Mineralogica Sinica*. **27**, 335–341 (in Chinese with English abstract).

Zhang Hai, Fang Weixuan, Zhang Guishan, Gan Fengwei, Wei Ning, and Guo Yuqian (2009) Facies sequence reestablishment and metallogenic analysis of Middle Triassic Anisian meta-volcanic rocks in the Kafang ore district, Gejiu, Yunnan [J]. *Geology in China.* **36**, 1322–1330 (in Chinese with English abstract).

Zhang Yin, Huang Zhilong, Luo Taiyi, and Qian Zhikuan (2011) LA-ICP-MS zircon U-Pb dating and petrogenesis of Shenxianshui granite in Gejiu, Yunnan Province, China [J]. *Acta Mineralogica Sinica.* **31**, 515–523 (in Chinese with English abstract).

Zhuang Yongqiu, Wang Renzhong, Yang Shupei, and Yin Jinming (1996) *Gejiu Sn-Cu Multimetal Ore Deposits of Yunnan* [M]. pp.202. Seismological Press, Beijing (in Chinese).